Nano Antenna Array for Terahertz Detection

Mario Bareiß, Badri N. Tiwari, Andreas Hochmeister, Gunther Jegert, Ute Zschieschang, Hagen Klauk, *Member, IEEE*, Bernhard Fabel, Giuseppe Scarpa, Gregor Koblmüller, Gary H. Bernstein, *Fellow, IEEE*, Wolfgang Porod, *Fellow, IEEE*, and Paolo Lugli, *Fellow, IEEE*

***Abstract*—Infrared (IR) detectors have been fabricated consisting of antenna-coupled metal–oxide–metal diodes (ACMOMDs). These detectors were defined using electron beam lithography with shadow evaporation metal deposition. They are designed to be sensitive to the IR range and work at room temperature without cooling or biasing. In order to achieve large arrays of ACMOMDs, nanotransfer printing have been used to cover a large area with metal–oxide–metal (MOM) diodes and with antenna structures. The printed antenna structures consist of gold and aluminum and exhibit a low electrical resistivity. A large area array of MOM tunneling diodes with an ultrathin dielectric (~3.6-nm aluminum oxide) has also been fabricated via the transfer-printing process. The MOM diodes exhibit excellent tunneling characteristics. Both direct and Fowler–Nordheim tunneling has been observed over eight orders of magnitude in current density. Static device parameters have been extracted via kinetic Monte Carlo simulations and have confirmed the existence of a dipole layer at the aluminum/aluminum oxide interface of the printed tunneling diodes. The mechanical yield of the transfer-printing process for the MOM tunneling diodes is almost a 100%, confirming that transfer printing is suitable for large area effective fabrication of these quantum devices.**

***Index Terms*—Antenna arrays, infrared (IR) detectors, metal–oxide–metal (MOM) techniques, quantum devices, rectennas, terahertz optoelectronics.**

I. Introduction

INFRARED detectors are important devices in e.g., security and medical fields. Antenna-coupled metal–oxide–metal diodes (ACMOMDs) are a promising candidate for infrared (IR) detectors due to their small size, CMOS compatibility, and ability to offer full functionality without cooling or applied bias [1]–[4]. The concept of ACMOMD was first introduced in the 1970s [5]–[7]. The device consists of two main components: the dipole antenna for receiving electromagnetic waves in a certain wavelength range and a metal–oxide–metal (MOM) diode that serves as the rectifying device. By varying the size of the dipole antenna, the sensitivity to a certain wavelength can be achieved. A dipole antenna length of several tenths of micrometers corresponds to the IR regime. The absorbed light induces a high-frequency ac current in the terahertz range, which is too fast for most electronic devices. Tunneling diodes are promising candidates for the rectification of terahertz signals because of the femtosecond tunneling times of an electron through a thin barrier in a MOM diode [8]. By selecting electrode metals with dissimilar work functions, the tunneling current through the thin dielectric becomes asymmetric with respect to the polarity of the voltage applied across the MOM diode, leading to the potential for excellent rectification at high frequencies [9], [10]. The thin dielectric layer must be on the order of a few nanometers to allow sufficiently large electrical current, and the area must be in the range of 50 nm $\times$ 50 nm to convert terahertz ac current into dc current [11]. Therefore, the MOM diode is the most challenging component of these detectors.

In Section II, the fabrication of ACMOMDs with electron beam lithography (EBL) techniques and the fabrication of antenna structures and MOM tunneling diodes over large areas in a nanotransfer-printing (nTP) process with both conventional and unconventional stamps. The electrical characterization of MOM tunneling diodes produced with EBL and with nTP techniques is presented in Section III, followed by the IR characterization of the EBL-defined ACMOMDs (Section IV).

II. Fabrication

A. Device Fabrication With EBL

High-frequency performance of ACMOMDs is limited by the *RC* time constant of the MOM diode. One way to lower this delay is to reduce the associated diode capacitance by fabricating thin lines on the order of 50 nm through EBL. We have developed two different EBL processes *viz.*: 1) a shadow evaporation technique that requires only one EBL step [1] and 2) a two-step lithography process in which two separate EBL exposures are performed with an intermediate step of oxide etching and regrowth [9]. The EBL has been performed using a 75-kV EBL system from Elionix Inc., Billerica, MA (ELS-7700). The substrate for these devices is a p-type Si (100) substrate with 1.5-μm thermally grown SiO_2.

The shadow evaporation technique is inspired from the Dolan offset mask process that was developed in 1977 at AT&T Bell Laboratories, Madison, WI [12]. In this technique, a bi-layer e-beam resist is used. In our process, the bottom layer is 400 nm

Manuscript received January 31, 2011; revised May 11, 2011; accepted May 24, 2011. Date of publication July 22, 2011; date of current version October 12, 2011. This work was supported in part by the Institute for Advanced Study and the International Graduate School for Science and Engineering of the Technische Universität München and by the DFG Excellence Cluster "Nanosystem Initiative Munich."

M. Bareiß, A. Hochmeister, G. Jegert, B. Fabel, G. Scarpa, and P. Lugli are with the Institute for Nanoelectronics, Technische Universität München (TUM), 81245 Munich, Germany (e-mail: bareiss@nano.ei.tum.de).

B. N. Tiwari, G. H. Bernstein, and W. Porod are with the Center for Nano Science and Technology, University of Notre Dame, Notre Dame, IN 46556 USA (e-mail: porod@nd.edu).

U. Zschieschang, and H. Klauk are with the Max Planck Institute for Solid State Research, 70569 Stuttgart, Germany (e-mail: H.Klauk@fkf.mpg.de).

G. Koblmüller is with the Walter Schottky Insitute, Technische Universität München (TUM), 80333 Garching, Germany (e-mail: Gregor.Koblmueller@wsi.tum.de).

Color versions of one or more of the figures in this paper are available online at http://ieeexplore.ieee.org.

Digital Object Identifier 10.1109/TMTT.2011.2160200

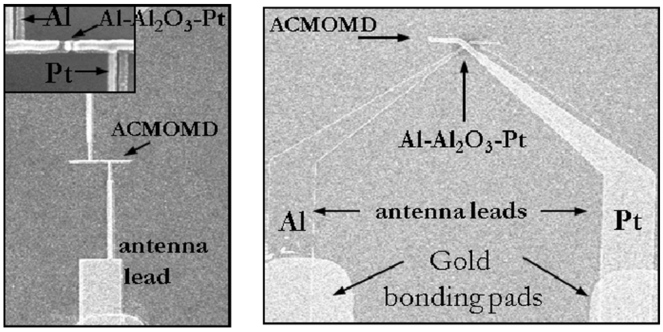

Fig. 1. SEM images of asymmetric barrier Al–Al_2O_3–Pt ACMOMDs. (a) Shadow evaporation device. The MOM overlap is shown in the inset. (b) Two-step lithography device. The MOM is formed where the antenna arms cross each other. The gold wire bonding pads are also seen where the antenna leads make contact.

of co-polymer methyl methacrylate (MMA-EL9, MicroChem, Newton, MA) and the top layer is 100 nm of less-sensitive poly methyl methacrylate (PMMA-C2, MicroChem). The first layer is flood exposed in ultraviolet (UV) light for 40 s. The UV exposure step is critically important in order to sufficiently remove the MMA after EBL exposure, leaving a PMMA bridge to facilitate double angle or shadow evaporation. Isopropyl alcohol (IPA), methyl isobutyl ketone (MIBK), and methyl ethyl ketone (MEK) are mixed in the ratio of 3:1:1.5% (vol.) [13] to prepare the PMMA developer. The bridge width should be approximately 40 nm to get a MOM overlap of 50 nm. The developed sample is mounted on a variable angle stage after de-scum in oxygen plasma using a PlasmaTherm RIE-790 etcher. Next, 30 nm of aluminum is deposited at an angle of $+7^\circ$ in an electron beam evaporator (FC 1800, Airco Temescal (now BOC Coating Technology), Suisun City, CA). *In situ* controlled oxidation of aluminum is performed to form Al_2O_3, which serves as the tunneling oxide, followed by 30 nm of platinum deposited at an angle of -7°. Although the oxide thickness has not been characterized, it is estimated to be 2–2.5 nm, which is sufficiently thin for tunneling of electrons [14]. Fig. 1(a) shows the completed shadow evaporation, or one-step EBL ACMOMD. The MOM overlap is also shown in the inset. The antenna is 3.1-μm long and $\sim$50-nm wide, and the MOM overlap is $\sim$50 nm $\times$ 50 nm.

The shadow evaporation technique uses controlled oxidation, and hence is limited to insulators that are native oxides of metals. To provide options for using different type of insulators and/or multiple insulator layers, a two-step lithography technique has been developed [3], [9], [15]–[17]. In this process, antenna arms and corresponding antenna leads are fabricated in two separate EBL steps. The antenna arms overlap and cross each other forming the MOM diode. Both of the EBL steps use the bi-layer e-beam resists to facilitate liftoff. First, the antenna arm and lead are metallized with 30 nm of aluminum. After development and de-scum of the EBL for the second antenna arm and lead, the sample is placed in the e-beam evaporator for *in situ* oxide etching using an end-Hall gridless ion source. The oxide regrowth is done using the *in situ* controlled oxidation of the etched surface of aluminum. Next, 30 nm of platinum is deposited following the controlled oxidation of aluminum. An ACMOMD realized with the two-step EBL ACMOMD is shown in Fig. 1(b).

B. Device Fabrication With nTP Process

The fabrication of ACMOMD with EBL technology in combination with natural oxidation and lift-off techniques shows very promising performance. In anticipation of the production of dense arrays of hundreds or thousands of tunneling diodes for imaging devices, an alternative fabrication method was developed, namely, direct transfer printing. A single metal layer [18] or a stack of different materials (e.g., metals and insulators [19], [20]) was prepared on a stamp and then transferred onto a target substrate. Up to now, only stacks with thicknesses in the range of several tens of nanometers have been realized and transferred [21]. For the fabrication of a MOM diode, thinner oxides down to a few nanometers are needed to permit large quantum-tunneling current densities [22], [23]. Furthermore, the antenna arms must have a thickness of 50 nm or less. This can be easily achieved using a stamp fabricated by a molecular beam epitaxy (MBE) process.

The MBE stamp process starts with a superlattice of AlGaAs and GaAs grown on a GaAs wafer. A rectangular part of approximately 2 mm $\times$ 3 mm is then cut out of the wafer and the GaAs layers are selectively etched in the breakage edge with citric acid [see Fig. 2(a)]. The detailed fabrication method of the MBE stamp, as well as our nTP tool prototype for executing the transfer printing process are described elsewhere [24]. After etching, a layer of Au with thickness of, e.g., 15 nm followed by 4 nm Ti (that serves during the transfer process as an adhesion promoter) were deposited by thermal metal evaporation on the edge of chip, which now serves as the stamp. By pressing the stamp for 30 s at a pressure of 300 MPa on a bare or oxidized Si substrate, the metal lines are transferred [see Fig. 2(b)]. We are also able to transfer other metals, such as aluminum, and to vary the film thickness. The electrical resistivity of the printed lines is in the same range than from bulk material.

The antenna array was printed in an MBE stamp process, whereas the MOM tunneling diode was fabricated in a transfer printing process using a conventional (flat) silicon wafer as a stamp. The silicon wafer covered with a hydrophobic organic self-assembled monolayer (SAM) of perflouroctyl–trichlorsilane as an antisticking. To create the hydrophobic SAM, the wafer is briefly exposed to an oxygen plasma (to create a density of hydroxyl groups sufficient for molecular self-assembly), placed for 30 min into a vacuum chamber along with 0.5 mL of perflouroctyltrichlorsilane at a pressure of 10 mbar, and then annealed at $\sim$140 °C on a hotplate. Due to the excellent stability of silane SAMs on silicon [25], [26], the stamp can be utilized repeatedly without damaging the antisticking SAM. The entire MOM tunneling diode is then created on the SAM-covered silicon stamp. First, a stack of 20-nm-thick gold followed by 30-nm-thick aluminum is deposited by vacuum evaporation through a shadow mask. This Au/Al stack later serves as the top electrode of the printed diode. The reason for depositing a stack of two different metals is that this makes it possible to choose a first metal (gold) that provides minimum adhesion to the fluoroalkyl SAM (to facilitate delamination from the stamp) and a

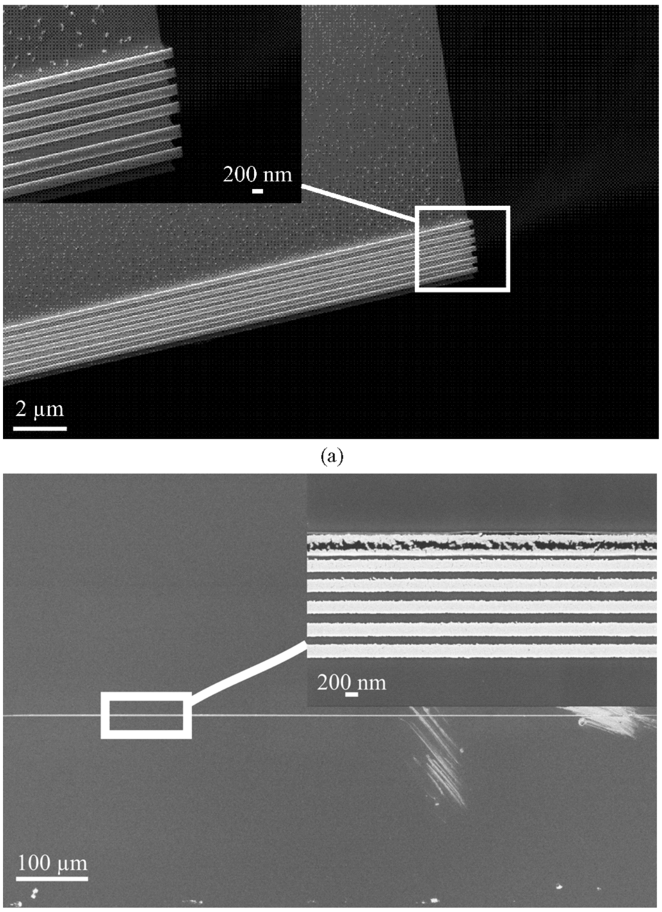

Fig. 2. (a) SEM image from MBE mold on the edge of a chip and (b) transfer-printed gold lines. The MBE mold in this structure consists of six layers of 200-nm-thick AlGaAs separated by 200-nm-thick layers of GaAs grown on a GaAs wafer. After etching GaAs selectively, the structure results in six free-standing AlGaAs-bars (clearly visible in the inset) on the edge of the chip. The transfer-printed lines extend in this figure over 800 μm. MBE stamps with structures down to 30 nm have been fabricated, and the experimental results are currently under investigation.

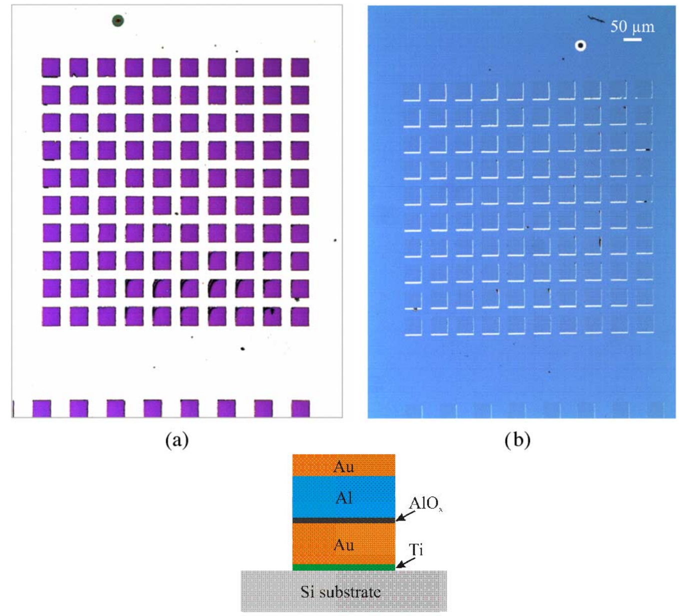

Fig. 3. Optical image of the: (a) top view of a part of the whole array of transfer-printed MOM tunneling diodes comprising a 3.6-nm-thick dielectric and (b) from the stamp after the transfer-printing process. Here, 100% of the diodes were transferred and some gold remained on the stamp at the corners. A cross section of the structure after transfer printing is shown in (c).

second metal (aluminum) that can be plasma oxidized to create a thin compact tunneling dielectric (AlO_x). This oxidation is performed by a brief oxygen–plasma treatment that increases the thickness of the native AlO_x layer on the aluminum surface from ~1.6 to ~3.6 nm [27], [28]. In the next step, a stack of 30-nm-thick gold (as the bottom electrode of the printed diode) followed by 4-nm-thick titanium (to promote adhesion of the printed diode to the target substrate) is deposited by vacuum evaporation through the same shadow mask. The titanium is allowed to oxidize and titanol surface groups are created by a UV and plasma treatment.

The completed diodes (Au/Al/AlO_x/Au/TiO_x) are then transfer printed onto the target substrate, namely, a silicon wafer covered with a 200-nm-thick layer of thermally grown silicon dioxide (Fig. 3). Transfer printing is performed using an Obducat NIL-2.5 Nanoimprinter at a temperature of 200 °C and a pressure of 50 bar for 5 min. During the transfer process, the titanol and silanol surface groups on the stamp and on the substrate react to titansiloxanes under water release [29]. This reaction is strongly promoted by drying the surfaces prior to transfer and removing physisorbed water from the interface at 200 °C during the printing process [30].

III. Electrical Characterization of MOM Diodes

A. Electron Beam Defined MOM Diodes

The fabricated ACMOMDs need to go through electrical characterizations to verify the nonlinear characteristics of the Al–Al_2O_3–Pt MOM diode. Since these are unbiased detectors, the quantities of interest are zero-biased resistance and zero-biased curvature coefficient, which are defined as

$$\text{zero-biased res.} = R_D^{\text{ZB}} = \left(\frac{dV}{dI}\right)_{V=0} \tag{1}$$

$$\text{zero-biasedcurv.coeff.} = \gamma_D^{\text{ZB}} = \left(\frac{\dfrac{d^2I}{dV^2}}{\dfrac{dI}{dV}}\right)_{V=0}. \tag{2}$$

DC voltage is swept from −300 to +300 mV and the current is measured. A polynomial fit is generated and first derivative of voltage at zero-bias (R_D^{ZB}) and the ratio of second derivative of current to the first derivative of current (γ_D^{ZB}) are derived. Fig. 4(a) shows a typical current–voltage (*I–V*) characteristic of an Al–Al_2O_3–Pt diode [1], [9]. As expected the *I–V* shows a nonlinear asymmetric variation, a very typical behavior of asymmetric Al–Al_2O_3–Pt diodes. In Fig. 4(b), variation of the curvature coefficient is shown for different bias voltages. Since these ACMOMDs are unbiased, for rectification of the IR radiation, there should be nonzero γ_D^{ZB} at zero bias $(V = 0)$.

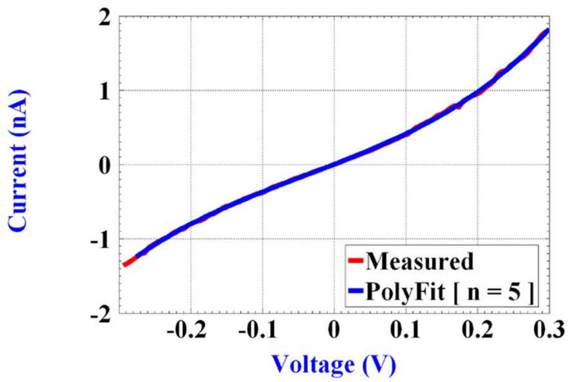

a)

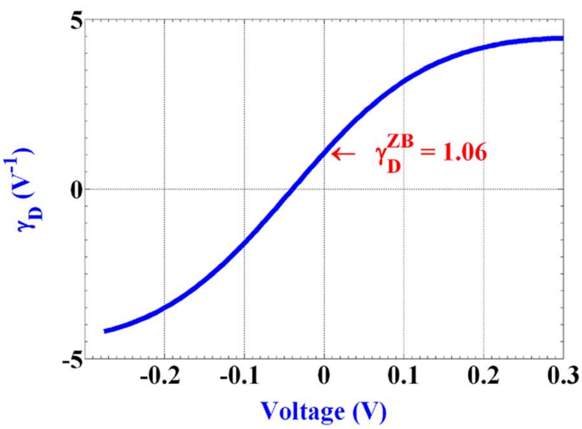

b)

Fig. 4. DC measurements of asymmetric barrier Al–Al_2O_3–Pt ACMOMDs. (a) Measured current in the voltage scan range of -300 to $+300$ mV and its fifth degree polynomial fit. (b) Variation of calculated curvature coefficient versus bias voltage. At zero bias, the curvature coefficient is nonzero, which is a required condition for unbiased ACMOMDs.

Typically, the values of $\gamma_D^{\rm ZB}$ for ACMOMDs have been found to be on the order of $\sim$1 per volt [1], [9].

B. Printed MOM Diodes

The total thickness of the MOM tunneling diodes before and after transfer printing was measured by atomic force microscopy (AFM), confirming the structural integrity of the transferred diodes, as the total thickness of the devices did not change upon transfer. The electrical characterization was done in the transfer-printed cross structure by contacting the printed top and bottom electrodes outside of the active diode area using probe needles and a parameter analyzer. The current through the 3.6-nm thin plasma-grown AlO_x dielectric was measured as a function of the applied bias on the gold bottom electrode. The aluminum top electrode was set to zero potential. The resulting *I–V* characteristic of a transfer-printed MOM diode is shown in Fig. 5, as well as the *I–V* characteristic of a reference MOM diode, which was fabricated by conventional thermal metal deposition (not transfer printed). Symbols and lines represent experimental data and theoretical values, respectively. Comparing the slope of the *I–V* curve of a transfer-printed tunneling diode with the reference diode, it can be seen that the electron transport mechanism

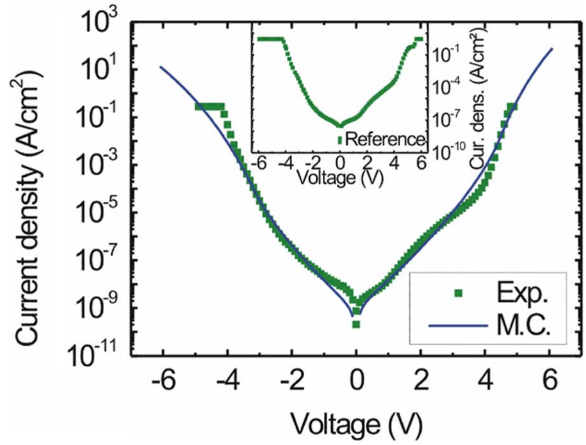

Fig. 5. Current density through a transfer-printed MOM tunneling diode measured as a function of applied voltage on the Au electrode. The lines represent the kinetic Monte Carlo simulation results using (1). In the inset, the *I–V* curve of a transfer-printed MOM tunneling diode is compared to that of a diode based on the same materials stack that was not transfer printed.

in both structures is identical. Furthermore, the current densities in the transfer-printed diode and in the reference diode are of the same order of magnitude, again confirming that the diodes are not damaged by the printing process. In order to identify the transport mechanism occurring in the MOM diodes, the measured current was modeled using a kinetic Monte Carlo simulator that encompasses models for the most relevant leakage current processes, e.g., quantum mechanical tunneling, thermionic emission, or trap-assisted tunneling [31], [32]. Direct tunneling of electrons through the oxide barrier was found to be the dominant transport mechanism due to the very small oxide thickness. Consequently, the current density j can be described analytically by the well-known Tsu–Esaki formula [33]

$$j = \frac{em_c k_B T}{2\pi^2\hbar^3} \int_0^\infty P(E_t) \ln \left[\frac{1+\exp\left(\dfrac{-E_t}{k_B T}\right)}{1+\exp\left(\dfrac{-eU-E_t}{k_B T}\right)} \right] dE_t \qquad (3)$$

where m_C is the conductivity mass for the injected electrons and $P(E_t)$ is the transmission coefficient for electrons with transversal energy E_t, calculated in the Wentzel–Kramers–Brillouin approximation. In the calculation of $P(E_t)$, an effective tunneling mass of $m_{\rm ox} = 0.38 m_0$ for the aluminum oxide, a tunneling barriers of 4.2 eV for the gold electrode, and 2.8 eV for the aluminum electrode have been taken. A good agreement with the experimental data is obtained, as shown in Fig. 5. The extracted barrier height of 4.2 eV corresponds to a gold/aluminum oxide interface in the Schottky limit, i.e., without any barrier reduction due to charge transfer across the interface [34]. Correspondingly, a barrier height of 3.2 eV would be expected for the aluminum barrier (taking $\Phi_{\rm Al} = 4.2$ eV), which is slightly larger than the extracted value of 2.8 eV. This discrepancy may be due to the formation of a dipole layer caused by charge transfer between the aluminum electrode and interfacial gap states in the aluminum oxide, which is known to reduce the barrier height [35]. Direct tunneling occurs for voltages between

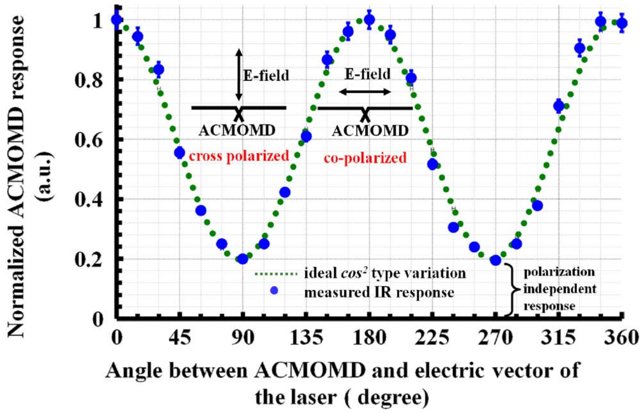

Fig. 6. IR response of ACMOMDs. It consists of a polarization-dependent part, which varies as $\cos^2$ and a polarization-independent response, which is believed to be of thermal origin. The device shows a polarization ratio of 5.

-4.2 V and $+2.8$ V on the gold electrode and Fowler–Nordheim tunneling takes place for higher absolute voltages. For current densities $|j| > 10^{-2}$ A/cm^2, irreversible degradation of the tunneling diode during the measurement, and finally, short circuiting, was observed.

IV. IR Characterization of ACMOMD

All of the ACMOMDs, fabricated through either the evaporation technique or the two step EBL technique that pass the dc test of showing nonzero curvature coefficient are subjected to IR characterization for full detector functionality. A linearly polarized continuous wave (CW) CO_2 laser (Lasy4G-SWT, Access Laser Company) has been used as the IR source. The shape of the IR beam has been characterized through the knife-edge experiment and the $1/e^2$ beamwidth was found to be ~4 mm. The laser beam passes through a polarizer, mechanical chopper, and a half-wave plate before it hits the device-under-test, the ACMOMDs. The half-wave plate is used to rotate the polarization of the IR laser without changing the orientation of devices or the laser.

According to classical antenna theory, if the polarization of the IR laser is rotated with respect to the orientation of the ACMOMD, the IR response of the ACMOMD should show a cosine-squared behavior [36], i.e., if δ_{IR} is the angle between the orientation of the ACMOMD and the electric field vector, the IR response should follow $|\cos(\delta_{\mathrm{IR}})|^2$ type variation. The IR response of ACMOMDs consists of polarization-dependent response that is varying cosine squared, as discussed, and the polarization-independent response, which is believed to be of thermal origin [16], [17]. In a co-polarized condition, the electric field is fully aligned with the ACMOMD, and in a cross-polarized condition, the electric field vector is perpendicular to the ACMOMD orientation. The ratio of the corresponding IR responses of the co-polarized and cross-polarized conditions gives the polarization ratio of an ACMOMD. A typical IR response of an ACMOMD is shown in Fig. 6. It is seen that the polarization-dependent signal is cosine squared varying with a dc offset provided by the polarization-independent signal. The polarization ratio for this ACMOMD is ~5. Presence of a polarization-dependent component in the IR response of the ACMOMDs shows that ACMOMDs behave as classical antennas and their radiation characteristics and other antenna parameters are governed by classical antenna theory.

V. Conclusion and Outlook

In summary, we have reported on the fabrication and characterization of IR detectors consisting of ACMOMDs. Two different processes comprising the EBL and the nTP technique have been described in detail to fabricate these detectors. The MOM diodes defined with EBL show unsymmetrical behavior, which is suitable to rectify high-frequency ac current into direct current. The transfer-printed MOM tunneling diodes with the oxygen-plasma-grown aluminum–oxide dielectric have shown that the dielectric retains its high quality during the transfer-printing process. Tunnel currents have been measured over eight orders of magnitude, including the transition from direct tunneling to Fowler–Nordheim tunneling. By comparison to a theoretical tunneling model, the static electronic properties of the diodes, i.e., the tunneling barrier heights and the tunneling effective mass, have been determined. As the mechanical yield of the transfer-printing process is almost 100%, we believe that transfer printing is an efficient and economical process to cover large areas with rectifying MOM tunneling diodes without affecting their electrical performance. Polarization-dependent measurements shows a $|\cos(\delta_{\mathrm{IR}})|^2$ type variation of the IR response, which proves that ACMOMDs behave as classical antennas. In future work, we will focus on the fabrication of large arrays of complete ACMOMDs with the nTP technique.

References

[1] J. A. Bean, B. Tiwari, G. H. Bernstein, P. Fay, and W. Porod, "Thermal infrared detection using dipole antenna-coupled metal–oxide–metal diodes," *J. Vac. Sci. Technol. B, Microelectron. Nanometer Struct.*, vol. 27, pp. 11–14, 2009.

[2] I. Codreanu, F. J. Gonzalez, and G. D. Boreman, "Detection mechanisms in microstrip dipole antenna-coupled infrared detectors," *Infrared Phys. Technol.*, vol. 44, pp. 155–163, 2003.

[3] C. Fumeaux, W. Herrmann, H. Rothuizen, P. De Natale, and F. K. Kneubühl, "Mixing of 30 THz laser radiation with nanometer thin-film Ni–NiO–Ni diodes and integrated bow-tie antennas," *Appl. Phys. B, Lasers Opt.*, vol. 63, pp. 135–140, 1996.

[4] P. Hobbs, R. Laibowitz, and F. Libsch, "Ni–NiO–Ni tunnel junctions for terahertz and infrared detection," *Appl. Opt.*, vol. 44, pp. 6813–6822, 2005.

[5] M. Heiblum, W. Shihyuan, J. Whinnery, and T. Gustafson, "Characteristics of integrated MOM junctions at dc and at optical frequencies," *IEEE J. Quantum Electron.*, vol. 14, pp. 159–169, 1978.

[6] M. Heiblum, S. Y. Wang, T. K. Gustafson, and J. R. Whinnery, "IIb-7 edge-MOM diode: An integrated, optical, non-linear device," *IEEE Trans. Electron. Devices*, vol. ED-24, no. 9, pp. 1199–1199, Sep. 1977.

[7] S. Y. Wang, T. Izawa, and T. K. Gustafson, "Coupling characteristics of thin-film metal–oxide–metal diodes at 10.6 μm," *Appl. Phys. Lett.*, vol. 27, pp. 481–483, 1975.

[8] J. A. Bean, A. Weeks, and G. D. Boreman, "Performance optimization of antenna-coupled Al/AlOx/Pt tunnel diode infrared detectors," *IEEE J. Quantum Electron.*, vol. 47, pp. 126–135, 2011.

[9] B. Tiwari, J. A. Bean, G. Szakmany, X. , G. H. Bernstein, P. Fay, and W. Porod, "Controlled etching and regrowth of tunnel oxide for antenna-coupled metal–oxide–metal diodes," *J. Vac. Sci. Technol. B, Microelectron. Nanometer Struct.*, vol. 27, pp. 2153–2160, 2009.

[10] J. A. Russer, P. Lugli, M. Bareiß, Y. Kuznetsov, W. Porod, H. Yordanov, and R. Russer, "Si and SiGe based monolithic integrated antennas for electromagnetic sensors and for wireless communications," in *Proc. 11th Silicon Monolithic Integr. Circuits RF Syst. Top. Meeting*, Phoenix, AZ, 2011, pp. 189–192.

[11] J. Bean, B. Tiwari, G. H. Bernstein, P. Fay, and W. Porod, "Long-wave infrared detection using dipole antenna-coupled metal–oxide–metal diodes," in *IEEE Silicon Nanoelectron. Workshop*, 2008, pp. 1–2.

[12] G. J. Dolan, "Offset masks for lift-off photoprocessing," *Appl. Phys. Lett.*, vol. 31, pp. 337–339, 1977.

[13] G. H. Bernstein and D. A. Hill, "On the attainment of optimum developer parameters for PMMA resist," *Superlattices Microstruct.*, vol. 11, pp. 237–240, 1992.

[14] M. E. Day, M. Delfino, and S. Salimian, "Low energy ion etching of aluminum oxide films and native aluminum oxide," *J. Appl. Phys.*, vol. 72, pp. 5467–5470, 1992.

[15] C. Fumeaux, G. D. Boreman, W. Herrmann, F. K. Kneubühl, and H. Rothuizen, "Spatial impulse response of lithographic infrared antennas," *Appl. Opt.*, vol. 38, pp. 37–46, 1999.

[16] I. Wilke, Y. Opplinger, W. Herrmann, and F. K. Kneubuhl, "Nanometer thin-film Ni–NiO–Ni diodes for 30 THz radiation," *Appl. Phy. A*, vol. 58, pp. 329–341, 1994.

[17] C. Fumeaux, W. Herrmann, F. K. Kneubühl, and H. Rothuizen, "Nanometer thin-film Ni–NiO–Ni diodes for detection and mixing of 30 THz radiation," *Infrared Phys. Technol.*, vol. 39, pp. 123–183, 1998.

[18] S. Harrer, S. Strobel, G. Scarpa, G. Abstreiter, M. Tornow, and P. Lugli, "Room temperature nanoimprint lithography using molds fabricated by molecular beam epitaxy," *IEEE Trans. Nanotechnol.*, vol. 7, no. 3, pp. 363–370, May 2008.

[19] Y.-L. Loo, D. V. Lang, J. A. Rogers, and J. W. P. Hsu, "Electrical contacts to molecular layers by nanotransfer printing," *Nano Lett.*, vol. 3, pp. 913–917, 2003.

[20] J. Zaumseil, M. A. Meitl, J. W. P. Hsu, B. R. Acharya, K. W. Baldwin, Y.-L. Loo, and J. A. Rogers, "Three-dimensional and multilayer nanostructures formed by nanotransfer printing," *Nano Lett.*, vol. 3, pp. 1223–1227, 2003.

[21] Y.-L. Loo, R. L. Willett, K. W. Baldwin, and J. A. Rogers, "Interfacial chemistries for nanoscale transfer printing," *J. Amer. Chem. Soc.*, vol. 124, pp. 7654–7655, 2002.

[22] T. W. Hickmott, "Defect conduction bands, localization, and temperature-dependent electron emission from $Al–Al_2O_3–Au$ diodes," *J. Appl. Phys.*, vol. 108, pp. 093703–093708, 2010.

[23] J. G. Simmons, "Generalized formula for the electric tunnel effect between similar electrodes separated by a thin insulating film," *J. Appl. Phys.*, vol. 34, pp. 1793–1803, 1963.

[24] P. Lugli, S. Harrer, S. Strobel, F. Brunetti, G. Scarpa, M. Tornow, and G. Abstreiter, "Advances in nanoimprint lithography," in *Proc. 7th IEEE Nanotechnol. Conf.*, 2007, pp. 1179–1184.

[25] W. Lee, R. Ji, C. A. Ross, U. Gösele, and K. Nielsch, "Wafer-scale Ni imprint stamps for porous alumina membranes based on interference lithography," *Small*, vol. 2, pp. 978–982, 2006.

[26] P. Russer, N. Fichtner, P. Lugli, W. Porod, J. A. Russer, and H. Yordanov, "Nanoelectronics-based integrate antennas," *IEEE Microw. Mag.*, vol. 11, pp. 58–71, 2010.

[27] U. Zschieschang, F. Ante, M. Schlörholz, M. Schmidt, K. Kern, and H. Klauk, "Mixed self-assembled monolayer gate dielectrics for continuous threshold voltage control in organic transistors and circuits," *Adv. Mater.*, vol. 22, pp. 4489–4493, 2010.

[28] H. Ryu *et al.*, "Logic circuits based on individual semiconducting and metallic carbon-nanotube devices," *Nanotechnology*, vol. 21, 2010, Art. ID 475207.

[29] G. Kissinger and W. Kissinger, "Hydrophilicity of silicon wafers for direct bonding," *Phys. Status Solidi (a)*, vol. 123, pp. 185–192, 1991.

[30] J. H. Anderson, Jr. and K. A. Wickersheim, "Near infrared characterization of water and hydroxyl groups on silica surfaces," *Surface Sci.*, vol. 2, pp. 252–260, 1964.

[31] G. Jegert, A. Kersch, W. Weinreich, U. Schroder, and P. Lugli, "Modeling of leakage currents in high-kappa dielectrics: Three-dimensional approach via kinetic Monte Carlo," *Appl. Phys. Lett.*, vol. 96, 2010, Art. ID 062113-3.

[32] G. Jegert, A. Kersch, W. Weinreich, and P. Lugli, "Monte Carlo simulation of leakage currents in $TiN/ZrO_2/TiN$ capacitors," *IEEE Trans. Electron Devices*, accepted for publication.

[33] R. Tsu and L. Esaki, "Tunneling in a finite superlattice," *Appl. Phys. Lett.*, vol. 22, pp. 562–564, 1973.

[34] J. Robertson, "Band offsets of wide-band-gap oxides and implications for future electronic devices," *J. Vac. Sci. Technol. B, Microelectron. Nanometer Struct.*, vol. 18, no. 3, pp. 1785–1791, 2000.

[35] J. Robertson, "Band offsets and work function control in field effect transistors," *J. Vac. Sci. Technol. B, Microelectron. Nanometer Struct.*, vol. 27, no. 1, pp. 277–285, 2009.

[36] C. A. Balanis, *Antenna Theory: Analysis and Design*. Hoboken, NJ: Wiley, 2005.

Mario Bareiß was born in Hagen, Germany. He received the Dipl.-Phys. degree in physics from the Technische Universität in München (TUM), Munich, Germany, in 2009, and is currently working toward the Ph.D. degree in physics at the Institute for Nanoelectronics, TUM. His Dipl.-Phys. research concerned InAs quantum dots on InP substrate fabricated with MBE for the application of a single photon source.

His current research interests include the fabrication of nanodevices with a special focus on the fabrication technology of nanoimprint lithography and nTP.

Badri N. Tiwari was born in Kanpur, India. He received the Bachelor of Technology (B.Tech.) degree in electronics and communication engineering from the Institute of Technology, Banaras Hindu University (IT-BHU), Varanasi, India, in 2003, the Master of Science (M.S.) degree in electrical engineering from the University of Notre Dame (UND), Notre Dame, IN, in 2007, and is currently working toward the Ph.D. degree at UND. He worked for two years ('03,–'05) in Defense Avionics Research Establishment (DARE), Bangalore, India as a Radio Frequency (RF) Scientist.

In 2005, he joined UND, where he has been involved with the design, fabrication, and characterization of antenna detection based IR sensors. His research interests include MOM diode and thermoelectric effect based sensors, high-frequency antenna design and simulation, thermal modeling of passives, nanofabrication, and electrical and optical characterization.

Andreas Hochmeister is currently doing working toward his Diploma degree in physics at the Institute for Nanoelctronics, Technische Universität München (TUM), Munich, Germany. His Diploma thesis concerns the fabrication and direct transfer printing of MOM diodes.

Gunther Jegert was born in Usingen, Germany, in 1981. He received the Dipl.-Phys. degree in physics from the Technische Universität München (TUM), Munich, Germany, in 2007, and is currently working toward the Ph.D. degree in physics at the Institute for Nanoelectronics, TUM. His Dipl.-Phys. research concerned GaN quantum dots as optical transducers for chemical sensors.

His research focuses on the modeling and simulation of transport in nanostructures and reliability analysis in high-k dielectrics. His current interests also involve the simulation of photocurrent generation in organic solar cells.

Ute Zschieschang received the Diplomingenieur degree in mechanical engineering from the Mittweida University of Applied Sciences, Mittweida, Germany, in 2000, and the Ph.D. degree in chemistry from the Technical University Bergakademie Freiberg, Freiberg, Germany, in 2006.

Since 2005, she has been a Scientist with the Organic Electronics Group, Max Planck Institute for Solid State Research, Stuttgart, Germany. Her research interests include high-performance conjugated semiconductors, SAMs, and micropatterning techniques for organic devices and circuits.

Hagen Klauk (S'97–M'99) received the Diplomingenieur degree in electrical engineering from the Chemnitz University of Technology, Chemnitz, Germany, in 1995, and the Ph.D. degree in electrical engineering from the Pennsylvania State University, University Park, in 1999.

From 1999 to 2000, he was a Postdoctoral Researcher with the Center for Thin Film Devices, Pennsylvania State University. In 2000, he joined Infineon Technologies, Erlangen, Germany. Since 2005, he has been Head of the Organic Electronics Group, Max Planck Institute for Solid State Research, Stuttgart, Germany. His research is focused on flexible transistors and circuits based on organic semiconductors, carbon nanotubes, and inorganic semiconductor nanowires.

Bernhard Fabel was born in Teheran, Iran. He received the Diploma (Dipl.-Ing.) degree in electrical engineering and Doctoral degree (Dr.-Ing) from the Technische Universität München (TUM), Munich, Germany, in 2004 and 2010, respectively.

He is currently a Research Assistant with the Institute of Nanoelectronics, TUM. His current research interest is in printable nanoscaled electronics and organic devices.

Giuseppe Scarpa recevied the M.Sc. degree in electrical engineering from the University of Rome "Tor Vergata," Rome, Italy, in 1998, the Ph.D. degree from the Walter Schottky Institute, Technical University of Munich, Garching, Germany, in 2003, and the Habilitation degree in the fields of nanoelectronics and molecular electronics from the Institute for Nanoelectronics, Technische Universität München (TUM), Munich, Germany, in 2009.

He is currently with the Institute for Nanoelectronics, TUM. He was engaged in research on design and fabrication of quantum cascade lasers. His current research interests include fabrication of a variety of nanostructures (such organic devices and nanomagnets) and the development of various nanofabrication technologies based on nanoimprint lithography.

Gregor Koblmüller received the M.Sc. and Ph.D. degrees in physics from the Vienna University of Technology (TU Wien), Vienna, Austria, in 2002 and 2005, respectively.

During his M.S. and Ph.D. thesis, he performed all his experimental work with the Corporate Research Division, Infineon Technologies AG, Munich, Germany. In 2005, he became a Postdoctoral Researcher and Project Scientist with the Materials Department, University of California at Santa Barbara (UCSB). In 2009, he joined the Walter Schottky Institute, Technische Universität München (TUM), Garching, Germany, as Group Leader for III–V semiconductor materials, where his current research focuses on epitaxial integration of III–arsenide nanostructures and heterostructures (quantum dots, nanowires) on silicon, the fabrication of ultrahigh mobility electron gases, and nanofabrication of sub-nanometer pattern for organic and molecular electronics.

Dr. Koblmüller was the recipient of several awards, including the IUPAP Young Author Best Paper Award and the Young Investigator MBE Award 2010.

Gary H. Bernstein (S'78–M'79–SM'95–F'06) received the B.S.E.E. degree (with honors) from the University of Connecticut, Storrs, in 1979, the M.S.E.E. degree from Purdue University, West Lafayette, IN, in 1981, and the Ph.D. degree in electrical engineering from Arizona State University, Tempe, in 1987.

In 1988, he joined the University of Notre Dame, Notre Dame, IN, and was the Founding Director of the Notre Dame Nanoelectronics Facility (from 1989 to 1998). In 1998, he became a Professor. From 1999 to 2006, he was the Associate Chairman of his department. He has authored or coauthored over 200 publications in the areas of electron-beam lithography, quantum electronics, high-speed integrated circuits, electromigration, microelectromechanical systems (MEMS), and electronics packaging.

Dr. Bernstein was the recipient of a National Science Foundation (NSF) White House Presidential Faculty Fellowship in 1992. He was also the lead-author recipient of the IEEE TRANSACTIONS ON ADVANCED PACKAGING Best Paper of the Year in 2007.

Wolfgang Porod (M'86–SM'90–F'02) received the Diplom (M.S.) and Ph.D. degrees from the University of Graz, Graz, Austria, in 1979 and 1981, respectively.

Following appointments as a Postdoctoral Fellow with Colorado State University and as a Senior Research Analyst with Arizona State University, he joined the University of Notre Dame, Notre Damn, IN, in 1986, as an Associate Professor. He is currently the Frank M. Freimann Professor of Electrical Engineering with the University of Notre Dame. He is also currently the Director of the Center for Nano Science and Technology, University of Notre Dame. He has authored or coauthored some 300 publications and presentations. His research interests are in the area of nanoelectronics with an emphasis on new circuit concepts for novel devices.

Dr. Porod has served as the Vice President for Publications for the IEEE Nanotechnology Council (2002–2003). He was an associate editor for the IEEE TRANSACTIONS ON NANOTECHNOLOGY (2001–2005). He has been active on several committees, in organizing special sessions and tutorials, and as a speaker for IEEE Distinguished Lecturer programs.

Paolo Lugli (F'10) received the Laurea degree in physics from the University of Modena, Modena, Italy, in 1979, and the M.Sc. and Ph.D. degrees in electrical engineering from Colorado State University, Fort Collins, in 1982 and 1985, respectively.

In 1993, he became a Full Professor of optoelectronics with the Universita di Roma "Tor Vergata," Rome, Italy. Since 2002 he has been with the Technische Universität München (TUM), Munich, Germany, as the Head of the newly created Institute for Nanoelectronics. His current interests involve modeling and simulation of nanostructures, as well as the realization and characterization of organic devices.